

ENTROPY-GUIDED AGREEMENT-DIVERSITY: A SEMI-SUPERVISED ACTIVE LEARNING FRAMEWORK FOR FETAL HEAD SEGMENTATION IN ULTRASOUND

Fangyijie Wang^{*†○} Siteng Ma[†] Guénolé Silvestre^{††} Kathleen M. Curran^{†○}

[†] Taighde Éireann – Research Ireland Centre for Research Training in Machine Learning, Ireland

[†] School of Computer Science, University College Dublin, Ireland

[○] School of Medicine, University College Dublin, Ireland

ABSTRACT

Fetal ultrasound (US) data is often limited due to privacy and regulatory restrictions, posing challenges for training deep learning (DL) models. While semi-supervised learning (SSL) is commonly used for fetal US image analysis, existing SSL methods typically rely on random limited selection, which can lead to suboptimal model performance by overfitting to homogeneous labeled data. To address this, we propose a two-stage Active Learning (AL) sampler, Entropy-Guided Agreement-Diversity (EGAD), for fetal head segmentation. Our method first selects the most uncertain samples using predictive entropy, and then refines the final selection using the agreement-diversity score combining cosine similarity and mutual information. Additionally, our SSL framework employs a consistency learning strategy with feature down-sampling to further enhance segmentation performance. In experiments, SSL-EGAD achieves an average Dice score of 94.57% and 96.32% on two public datasets for fetal head segmentation, using 5% and 10% labeled data for training, respectively. Our method outperforms current SSL models and showcases consistent robustness across diverse pregnancy stage data. The code is available on GitHub.

Index Terms— Semi-supervised Learning, Active Learning, Fetal US, Segmentation

1. INTRODUCTION

Ultrasound (US) imaging is extensively utilized for prenatal assessment of fetal growth, fetal anatomy, estimating gestational age, and monitoring pregnancy due to its portability, affordability, and non-invasive nature [1, 2]. In particular, the analysis of anatomical structures is a critical component of fetal screening as it provides direct evidence of potential fetal malformations, placental localization disorders, and the risk of premature birth [1].

Deep learning (DL) has shown great potential for fetal US image analysis [3, 4]. However, robust models re-

quire extensive expert annotations, which are costly and time-consuming [5, 6]. A sufficient amount of expert annotations is crucial for developing robust DL algorithms. However, annotating US images is a labor-intensive and time-consuming process that demands medical proficiency and clinical expertise for accurate pixel-level labeling [5, 6]. Recent works [7, 8, 9] have applied semi-supervised learning (SSL) to this field, yet existing methods still struggle with accurate fetal anatomical segmentation, highlighting the need for tailored SSL approaches.

Moreover, current SSL methods typically rely on fixed, randomly selected labeled samples. This often leads to insufficient model learning and introduces prediction-level noise, resulting in suboptimal segmentation performance for small fetal anatomical structures in early-stage ultrasound scans. In contrast, Active Learning (AL) is a machine learning paradigm that can iteratively query the most informative samples for labeling, thereby achieving performance comparable to fully supervised learning with minimal labeled data [10], and addressing the limitations above.

In this paper, we investigate the following research question: *Can the AL query strategy help SSL framework improve the segmentation performance of lightweight DL in US analysis?* To answer this question, we propose a novel approach named Entropy-Guided Agreement-Diversity strategy for Semi-Supervised Learning (SSL-EGAD) for fetal head segmentation in US. Unlike existing SSL methods, SSL-EGAD is the first algorithm to adapt AL query strategy based on the learning outcomes of the semi-supervised lightweight DL model. Our experiments demonstrate that SSL-EGAD outperforms the state-of-the-art (SOTA) methods in fetal head segmentation. This advancement facilitates a cost-effective reduction in labeling costs and enhances the robustness of models for various fetal anatomical segmentation scenarios.

2. METHODOLOGY

The overview of our method SSL-EGAD is shown in Fig. 1. Given a fetal US dataset, $(X_L \in \mathbb{R}^{3 \times n_h \times n_w}, Y_{gt} \in \mathbb{R}^{2 \times n_h \times n_w})$ denotes the initialized labeled training dataset that is randomly selected, while X_{UL} denotes the initialized unlabeled

* Corresponding author (fangyijie.wang@ucdconnect.ie)

This work was funded by Taighde Éireann – Research Ireland through the Centre for Research Training in Machine Learning (18/CRT/6183).

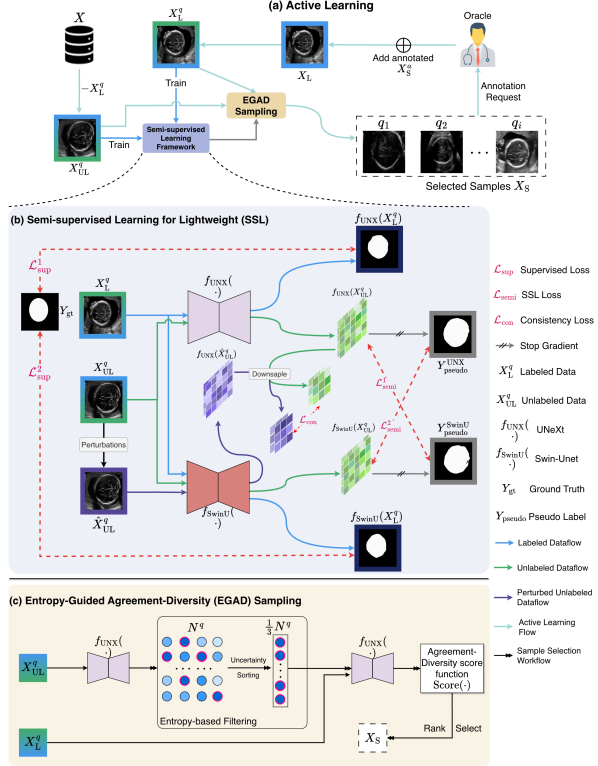


Fig. 1. An overview of our proposed SSL-EGAD with SwinUnet and UNeXt for fetal US image segmentation.

training dataset. $\mathbf{X}_L, \mathbf{X}_{UL} \in \mathbb{R}^{3 \times n_h \times n_w}$ represents a 2D fetal US image of size $n_h \times n_w$ with 3 channels. \mathbf{X}_L^i are selected samples with query strategy Q at each AL round i , see details in Section 2.1. We incorporate \mathbf{X}_S into the labeled set \mathbf{X}_L and exclude \mathbf{X}_S from the unlabeled set \mathbf{X}_{UL} to derive the sets \mathbf{X}_L^q and \mathbf{X}_{UL}^q , respectively. The sets \mathbf{X}_L^q and \mathbf{X}_{UL}^q are training data of SSL framework.

2.1. Entropy-Guided Agreement-Diversity Sampler

To efficiently identify the most informative unlabeled images for annotation, we propose an Entropy-Guided Agreement-Diversity (EGAD) Sampler, illustrated in Fig. 1(c). EGAD adopts a two-stage filter-refine strategy that balances model uncertainty and sample diversity, enabling label-efficient SSL. In the first stage, we measure the predictive uncertainty of each unlabeled image using the mean predictive entropy of the segmentation probabilities:

$$\mathcal{H}_j = - \sum_{c=1}^2 \sum_{h=1}^{n_h} \sum_{w=1}^{n_w} \mathbf{p}_{j,c,h,w} \log(\mathbf{p}_{j,c,h,w})$$

where $\mathbf{p}_j \in \mathbb{R}^{2 \times n_h \times n_w}$ is the model prediction. The top one-third of unlabeled samples with the highest entropy values are retained as uncertain candidates, ensuring that subsequent selection focuses on regions of the data space where the model exhibits high epistemic uncertainty. In the second

stage, EGAD evaluates each image among the uncertain candidates using a hybrid agreement-diversity score, which captures both semantic similarity in feature space and statistical dependence in image space. For an unlabeled image \mathbf{X}_{UL}^q and a labeled image \mathbf{X}_L^q , we compute:

$$\text{CosSim}(\mathbf{X}_{UL}^q, \mathbf{X}_L^q) = \frac{z(\mathbf{X}_L^q)^\top z(\mathbf{X}_{UL}^q)}{\|z(\mathbf{X}_L^q)\| \|z(\mathbf{X}_{UL}^q)\|}$$

where $z(\cdot)$ denotes the normalized feature embedding, and the empirical mutual information between the two image intensities is defined as:

$$\text{MI}(\mathbf{X}_{UL}^q, \mathbf{X}_L^q) = \sum_{i,j} p_{\mathbf{X}_{UL}^q \mathbf{X}_L^q}(i,j) \log \frac{p_{\mathbf{X}_{UL}^q \mathbf{X}_L^q}(i,j)}{p_{\mathbf{X}_{UL}^q}(i)p_{\mathbf{X}_L^q}(j)}$$

The joint distribution $p_{\mathbf{X}_{UL}^q \mathbf{X}_L^q}$ is estimated via a 2D histogram over the intensity pairs of corresponding pixels across all channels. Each term is normalized to $[0, 1]$ across the unlabeled pool, and the final score is:

$$\text{Score}(\mathbf{X}_{UL}^q) = \mathcal{N}(\text{CosSim}(\mathbf{X}_{UL}^q)) - \mathcal{N}(\text{MI}(\mathbf{X}_{UL}^q))$$

The top k samples with the highest scores are selected for annotation. We set k to be one-third. This choice balances uncertainty and efficiency, and EGAD relies on relative ranking rather than the exact threshold, consistent with prior AL practice. This two-stage sampling strategy identifies highly uncertain samples and then prioritizes those that are both semantically distinct and statistically independent from the labeled data, yielding a more diverse and informative annotation set. $\text{CosSim}(\cdot)$ and $\text{MI}(\cdot)$ capture complementary redundancy, with normalization ensuring a stable, model-agnostic ranking without explicit weighting.

2.2. Semi-supervised Learning via Co-Training

Our proposed SSL method consists of two key components: (1) A co-training strategy for UNeXt [11] and Swin-Unet [12], represented by $f_\theta^{\text{UNX}}(\cdot)$ and $f_\phi^{\text{Swin}}(\cdot)$, respectively. (2) A consistency learning method between two networks using pseudo labels, shown in Fig. 1(b).

We utilize UNeXt [11] to construct our lightweight CNN model denoted as $f_\theta^{\text{UNX}}(\cdot)$. The number of channels across each block in the encoder path is set to [32, 64, 128, 160, 256]. The $f_\phi^{\text{Swin}}(\cdot)$ is implemented using the tiny Swin-Unet architecture from work [12]. To fit the resolution of our input image, which is 448×448 , the shifted window size is set to 7. The bottleneck feature dimension is 768. We initialize our model using pre-trained weights [12]. Table 1 compares the profiles of UNeXt and Swin-Unet. The UNeXt shows superior lightweight and efficiency to Swin-Unet.

Building upon the foundation laid by the previous co-training method Cross Pseudo Supervision [13, 8], we introduce a simple yet powerful cross-supervision learning framework that incorporates consistency learning. This approach combines a compact CNN network with a Transformer-based network to boost their performance collaboratively. Given the

Table 1. CNN and Transformer models' profiles.

Model	Input Size	Param (M) \downarrow	GFLOPs \downarrow
Swin-Unet	448×448	27.15	71.17
UNeXt	448×448	1.47	7.03

unlabeled dataset \mathbf{X}_{UL}^q in AL round, the proposed framework produces two predictions: $f_{\theta}^{\text{UNX}}(\mathbf{X}_{\text{UL}}^q)$ and $f_{\phi}^{\text{Swin}}(\mathbf{X}_{\text{UL}}^q)$. The pseudo labels for the CPS strategy are generated by:

$$\tilde{Y}^{\text{UNX}} = f_{\text{OH}}(f_{\theta}^{\text{UNX}}(\mathbf{X}_{\text{UL}})) ; \tilde{Y}^{\text{Swin}} = f_{\text{OH}}(f_{\phi}^{\text{Swin}}(\mathbf{X}_{\text{UL}})) .$$

where f_{OH} represents a one-hot encoding function.

Inspired by existing studies [14, 15], we leverage consistency learning via image perturbation in training, shown in Fig. 1(b), which helps the $f_{\theta}^{\text{UNX}}(\cdot)$ learn more robust and discriminative features. Specifically, we add Gaussian noise to the unlabeled data \mathbf{X}_{UL}^q , where noise $\sim \mathcal{N}(0, \sigma^2)$ and $\sigma = 0.2$. The perturbed data $\hat{\mathbf{X}}_{\text{UL}}^q$ is input to model $f_{\phi}^{\text{Swin}}(\cdot)$ to obtain probability outputs $f_{\phi}^{\text{Swin}}(\hat{\mathbf{X}}_{\text{UL}}^q) \in \mathbb{R}^{2 \times n_h \times n_w}$.

We also observe that the fetal head size in the first trimester is smaller compared to the second or third trimester, resulting in a large proportion of background pixels in US images. The consistency of these background pixels is unessential for model training. Therefore, we adopt a downsampling layer $\mathcal{D}(\cdot)$ to filter out insignificant pixels in $f_{\phi}^{\text{Swin}}(\hat{\mathbf{X}}_{\text{UL}}^q)$ and $f_{\theta}^{\text{UNX}}(\mathbf{X}_{\text{UL}}^q)$, prioritizing the representation of the fetal head in the image. The output size of $\mathcal{D}(\cdot)$ is denoted as C_{ds} , so the output is expressed as: $\mathcal{D}(f_{\theta}^{\text{UNX}}(\mathbf{X}_{\text{UL}}^q)) \in \mathbb{R}^{2 \times C_{\text{ds}} \times C_{\text{ds}}}$ and $\mathcal{D}(f_{\phi}^{\text{Swin}}(\hat{\mathbf{X}}_{\text{UL}}^q)) \in \mathbb{R}^{2 \times C_{\text{ds}} \times C_{\text{ds}}}$. Furthermore, we normalize them in the channel dimension to induce sparsity in the features and enhance the model's resilience to perturbations. The consistency learning loss \mathcal{L}_{con} is defined as:

$$\mathcal{L}_{\text{con}} = \mathcal{M}(\mathcal{N}_{\text{L2}}(\mathcal{D}(f_{\theta}^{\text{UNX}}(\mathbf{X}_{\text{UL}}))) - \mathcal{N}_{\text{L2}}(\mathcal{D}(f_{\phi}^{\text{Swin}}(\hat{\mathbf{X}}_{\text{UL}}^q))))$$

where $\mathcal{M}(\cdot)$ is mean squared error and $\mathcal{N}_{\text{L2}}(\cdot)$ introduces L₂ regularization.

2.3. The Overall Training Loss

The overall training loss is a joint loss with three parts: the supervision loss \mathcal{L}_{sup} for the labeled data, the semi-supervision loss $\mathcal{L}_{\text{semi}}$, and consistency loss \mathcal{L}_{con} for the unlabeled data. All training losses are highlighted by a red dashed line in Fig. 1. Mathematically, the joint loss can be expressed as:

$$\mathcal{L}_{\text{total}} = (\mathcal{L}_{\text{sup}}^1 + \mathcal{L}_{\text{sup}}^2) + \lambda(\mathcal{L}_{\text{semi}}^1 + \mathcal{L}_{\text{semi}}^2) + \mathcal{L}_{\text{con}} \quad (1)$$

where λ represents the weighting factor for a Gaussian ramp-up function used exclusively for the unlabeled training set [16]. This Gaussian ramp-up function facilitates the gradual transition of $f_{\theta}^{\text{UNX}}(\cdot)$ and $f_{\phi}^{\text{Swin}}(\cdot)$ from being initialized with the labeled training set to prioritizing learning from the unlabeled training set. The λ is expressed as $\lambda = e^{-5 \times (1 - t_{\text{iter}}/t_{\text{Max Iter}})^2}$, where $t_{\text{iter}} = N_{\text{epoch}}/B$ and B stands for the batch size. $\mathcal{L}_{\text{sup}}^1$ and $\mathcal{L}_{\text{sup}}^2$ are the supervision

Table 2. The details of HC18 and ES-TCB datasets.

Name	Image Size	Train	Validation	Test
HC18	800×540	500	50	449
ES-TCB	959×661	342	50	289

losses for $f_{\theta}^{\text{UNX}}(\cdot)$ and $f_{\phi}^{\text{Swin}}(\cdot)$ based on the labeled data \mathbf{X}_{L} . \mathcal{L}_{sup} is a combination loss, as follows:

$$\begin{aligned} \mathcal{L}_{\text{sup}}^1 &= \mathcal{H}(f_{\theta}^{\text{UNX}}(\mathbf{X}_{\text{L}}), \mathbf{Y}_{\text{gt}}) + \mathcal{D}(f_{\theta}^{\text{UNX}}(\mathbf{X}_{\text{L}}), \mathbf{Y}_{\text{gt}}) \\ \mathcal{L}_{\text{sup}}^2 &= \mathcal{H}(f_{\phi}^{\text{Swin}}(\mathbf{X}_{\text{L}}), \mathbf{Y}_{\text{gt}}) + \mathcal{D}(f_{\phi}^{\text{Swin}}(\mathbf{X}_{\text{L}}), \mathbf{Y}_{\text{gt}}) \end{aligned} \quad (2)$$

$\mathcal{H}(\cdot)$ and $\mathcal{D}(\cdot)$ denote the Cross-Entropy (CE) loss and the standard Dice based coefficient (Dice) loss, respectively. The semi-supervision losses are computed using pseudo labels \tilde{Y}^{UNX} and \tilde{Y}^{Swin} during co-training between $f_{\theta}^{\text{UNX}}(\cdot)$ and $f_{\phi}^{\text{Swin}}(\cdot)$, respectively. Therefore, the loss is defined as:

$$\begin{aligned} \mathcal{L}_{\text{semi}}^1 &= \mathcal{H}(f_{\theta}^{\text{UNX}}(\mathbf{X}_{\text{UL}}), \tilde{Y}^{\text{Swin}}) + \mathcal{D}(f_{\theta}^{\text{UNX}}(\mathbf{X}_{\text{UL}}), \tilde{Y}^{\text{Swin}}) \\ \mathcal{L}_{\text{semi}}^2 &= \mathcal{H}(f_{\phi}^{\text{Swin}}(\mathbf{X}_{\text{UL}}), \tilde{Y}^{\text{UNX}}) + \mathcal{D}(f_{\phi}^{\text{Swin}}(\mathbf{X}_{\text{UL}}), \tilde{Y}^{\text{UNX}}) \end{aligned}$$

The consistency learning loss \mathcal{L}_{con} is explained in Section 2.2.

3. EXPERIMENTS AND RESULTS

3.1. Datasets

Two public fetal US image datasets for different scenarios are used to evaluate our proposed method. Both of them were acquired from healthy singleton pregnancies. **Spanish trans-cerebellum (ES-TCB)** dataset is acquired from two centers in Spain [17] when pregnant women are in their 2nd and 3rd trimesters undergoing routine examinations [17]. Students, experienced physicians, and radiologists annotated the region of interest (ROI) of the fetal head in all images. We use 681 annotated trans-cerebellum images to undertake our experiments. **HC18** images are captured by experienced sonographers utilizing two different US machines in the Netherlands [18]. We use 999 annotated images in this study. The annotations represent the ROI that best fits the circumference of the fetal head in each image. We use a 50:50 ratio for both datasets to split the data into training and test sets. In our experiments, we examine two scenarios with limited labeled data available: 5% and 10%. The number of images for training, validation, and testing is illustrated in Table 2. Data augmentation techniques are only applied to the labeled data during training. The detailed parameters of the data augmentation techniques are in our code repository on GitHub.

3.2. Benchmark Methods

We compare the segmentation performance of SSL-EGAD with the benchmark and SOTA methods in SSL field. There are nine SSL methods trained using the same hyperparameter settings. The test, labeled, and unlabeled training sets are randomly selected once and evaluated collectively with all methods. These SSL methods reported include: Mean Teachers

(MT) [14], Deep Co-Training (DCT) [19], Uncertainty-Aware Mean Teachers (UAMT) [15], Cross Pseudo Supervision (CPS) [13], Cross Teaching between CNN and Transformer (CTCT) [20], Lightweight Model for Contrastive Learning (LMCT) [9], and Pixel-level contrastive and cross-supervised (PCCS) [8]. For AL query strategy, we compare two of the most well-known and commonly used methods in the AL field, diversity-based (Random) and covering uncertainty-based (Entropy [10]).

3.3. Implementation Details and Evaluation Metrics

We trained each method with 400 epochs. With the query strategy, each AL iteration was trained with 400 epochs, and the max iterative loop was set to 5 to ensure fair comparison under equal annotation budgets. The labeled batch size is set to 1, the unlabeled batch size is set to 4, the optimizer is stochastic gradient descent (SGD), the learning rate is set to 0.01, momentum is 0.9, and weight decay is 0.0001. For AL, we set iteration $i = 5$. The size of X_S^i is 1% and 2% of the labeled data in the 5% and 10% scenarios, respectively. Our code is developed in Python 3.11.5 using Pytorch 2.1.2 and CUDA 12.2 using one NVIDIA 4090 GPU. In training, we evaluate the UNeXt model on the validation set every epoch and store the weights of the best-performing UNeXt model. All images are resized to dimensions of 448×448 pixels. The above setting is also applied to all other benchmark methods directly without any modification. For model evaluation, we utilize the following evaluation metrics: Dice Score (DSC), and difference measure: Hausdorff Distance (HD). We assess the performance of SSL-EGAD across scenarios involving 5% and 10% of labeled data for training.

3.4. Results

The quantitative results of fetal head segmentation are summarized in Table 3. The first two rows show the fully supervised baselines, UNeXt and Swin-Unet. Under both 5% and 10% labeled data settings, our proposed SSL-EGAD consistently surpasses all other SSL methods and AL strategies, while maintaining results comparable to the fully supervised Swin-Unet. It effectively bridges the gap between UNeXt and Swin-Unet, highlighting the ability of our approach to generate a robust, lightweight model by efficiently exploiting unlabeled data. Overall, the proposed EGAD strategy proves more effective than conventional active learning strategies such as Random and Entropy, yielding superior segmentation accuracy and boundary precision.

Ablation Study. We conducted an ablation study to analyze the contribution of each component in our framework using 5% labeled data from the HC18 dataset. As shown in Table 4, the SSL baseline surpasses the fully supervised model, indicating the benefit of leveraging unlabeled data. Comparing the second and third rows reveals that combining CNN and Transformer backbones leads to better feature representation than using dual CNN architectures. Incorpor-

Table 3. The quantitative results of SSL-EGAD (UNeXt) and other methods when 5% and 10% of label data for training. The best results are in **bold**.

Method	AL Strategy	# Labeled	HC18		ES-TCB	
			DSC \uparrow	HD \downarrow	DSC \uparrow	HD \downarrow
UNeXt Swin-Unet	N/A	100%	93.37	48.60	94.69	45.57
		100%	96.94	12.51	96.96	14.91
MT [14]		5%	89.43	59.26	90.81	58.83
DCT [19]			91.69	54.29	90.76	56.11
UAMT [15]			90.97	57.57	89.98	59.39
CPS [13]			91.35	58.51	91.42	51.15
CTCT [20]			91.50	54.26	90.88	53.38
PCCS [8]	Random Entropy EGAD	92.24	51.23	91.38	50.36	
LCMT [9]		93.24	46.90	92.70	47.38	
LCMT [9]		94.06	35.87	91.84	57.59	
CEAL [10]		94.07	41.13	94.50	48.82	
SSL-EGAD		95.09	28.77	94.04	41.43	
MT [14]	N/A	94.38	35.19	93.20	48.22	
DCT [19]		94.67	35.25	93.93	45.07	
UAMT [15]		94.86	32.93	93.07	50.90	
CPS [13]		94.61	33.60	92.79	50.15	
CTCT [20]		94.80	35.80	94.38	43.69	
PCCS [8]		95.13	29.80	94.83	44.11	
LCMT [9]		95.31	29.50	95.15	39.32	
LCMT [9]	Random	95.67	28.68	95.35	36.39	
CEAL [10]	Entropy	95.69	29.17	95.40	42.24	
SSL-EGAD	EGAD	96.44	19.15	96.21	25.74	

Table 4. Ablation study on the effectiveness of each component using 5% labeled data. The best results are in **bold**.

Method	Backbone	DSC \uparrow	
		HC18	ES-CB
Fully Supervised	UNeXt	38.79	81.24
SSL	Swin-Unet+UNeXt	88.85	88.40
SSL+ \mathcal{L}_{con}	UNeXt+UNeXt	85.88	87.73
SSL+ \mathcal{L}_{con}	Swin-Unet+UNeXt	93.22	92.95
SSL+ \mathcal{L}_{con} +EGAD	Swin-Unet+UNeXt	95.09	94.04

rating consistency learning (\mathcal{L}_{con}) further enhances segmentation performance, demonstrating its effectiveness in stabilizing training and improving generalization. Finally, integrating our proposed EGAD strategy yields the best results across both datasets, confirming its effectiveness in selecting informative samples and fully exploiting unlabeled data.

4. CONCLUSION

In this study, we propose SSL-EGAD, a framework integrating AL with SSL to overcome limitations of existing methods in fetal head segmentation. By guiding a lightweight model to focus on informative regions, SSL-EGAD improves structural understanding and generalization. Experiments show that SSL-EGAD achieves superior performance with minimal labeled data, reducing annotation costs while maintaining high accuracy in fetal head analysis. The EGAD strategy is task-agnostic and can be integrated with other SSL pipelines. Extending the framework to additional fetal structures and imaging modalities will be explored in future work.

5. COMPLIANCE WITH ETHICAL STANDARDS

This research study was conducted retrospectively using human subject data made available in open access by [18, 17]. Ethical approval was not required as confirmed by the license attached with the open access data.

6. REFERENCES

- [1] L. J. Salomon, Z. Alfirevic, V. Berghella, C. Bilardo, others, and on behalf of the ISUOG Clinical Standards Committee, “Practice guidelines for performance of the routine mid-trimester fetal ultrasound scan,” *Ultrasound in Obstetrics & Gynecology*, vol. 37, no. 1, pp. 116–126, 2011.
- [2] P. Zaffino, S. Moccia, E. De Momi, and M. F. Spadea, “A review on advances in intra-operative imaging for surgery and therapy: Imagining the operating room of the future,” *Annals of Biomedical Engineering*, vol. 48, no. 8, pp. 2171–2191, Aug. 2020.
- [3] S. Płotka, T. Włodarczyk, A. Kłasa, M. Lipa, A. Sitek, and T. Trzciński, “FetalNet: Multi-task deep learning framework for fetal ultrasound biometric measurements,” in *Neural Information Processing*. 2021, pp. 257–265, Springer.
- [4] R. Yasrab, H. Zhao, Z. Fu, L. Drukker, A. T. Pageorghiou, and J. A. Noble, “Automating the human action of First-Trimester biometry measurement from Real-World freehand ultrasound,” *Ultrasound in Medicine & Biology*, vol. 50, no. 6, pp. 805–816, 2024.
- [5] D. Piaggio, R. Castaldo, M. Cinelli, S. Cinelli, A. Maccaro, and L. Pecchia, “A framework for designing medical devices resilient to low-resource settings,” *Globalization and Health*, vol. 17, no. 1, pp. 64, 2021.
- [6] R. Ramirez Zegarra and T. Ghi, “Use of artificial intelligence and deep learning in fetal ultrasound imaging,” *Ultrasound in Obstetrics & Gynecology*, vol. 62, no. 2, pp. 185–194, 2023.
- [7] J. Jiang, H. Wang, J. Bai, S. Long, et al., “Intrapartum ultrasound image segmentation of pubic symphysis and fetal head using dual student-teacher framework with cnn-vit collaborative learning,” in *MICCAI*. October 2024, vol. LNCS 15001, Springer.
- [8] C. Ma and Z. Wang, “Semi-Mamba-UNet: Pixel-level contrastive and cross-supervised visual mamba-based UNet for semi-supervised medical image segmentation,” *Knowledge-Based Systems*, vol. 300, pp. 112203, Sept. 2024.
- [9] F. Wang, K. M. Curran, and G. Silvestre, “Semi-supervised cervical segmentation on ultrasound by a dual framework for neural networks,” in *IEEE 22nd International Symposium on Biomedical Imaging*, 2025.
- [10] K. Wang, D. Zhang, Y. Li, R. Zhang, and L. Lin, “Cost-effective active learning for deep image classification,” *IEEE Transactions on Circuits and Systems for Video Technology*, vol. 27, no. 12, pp. 2591–2600, 2017.
- [11] J. M. J. Valanarasu and V. M. Patel, “UNeXt: MLP-Based rapid medical image segmentation network,” in *MICCAI*. 2022, pp. 23–33, Springer.
- [12] H. Cao, Y. Wang, J. Chen, D. Jiang, et al., “Swin-UNet: Unet-Like pure transformer for medical image segmentation,” in *ECCV Workshops*. 2023, pp. 205–218, Springer.
- [13] X. Chen, Y. Yuan, G. Zeng, and J. Wang, “Semi-supervised semantic segmentation with cross pseudo supervision,” in *Proceedings of the IEEE/CVF Conference on Computer Vision and Pattern Recognition*, June 2021, pp. 2613–2622.
- [14] A. Tarvainen and H. Valpola, “Mean teachers are better role models: Weight-averaged consistency targets improve semi-supervised deep learning results,” in *NeurIPS*, 2017, vol. 30.
- [15] L. Yu, S. Wang, X. Li, C. Fu, and P. Heng, “Uncertainty-Aware self-ensembling model for semi-supervised 3D left atrium segmentation,” in *Medical Image Computing and Computer Assisted Intervention*. 2019, pp. 605–613, Springer.
- [16] S. Laine and T. Aila, “Temporal ensembling for semi-supervised learning,” in *International Conference on Learning Representations*, 2017.
- [17] M. Alzubaidi, M. Agus, M. Makhlof, F. Anver, K. Alyafei, and M. Househ, “Large-scale annotation dataset for fetal head biometry in ultrasound images,” *Data in Brief*, vol. 51, pp. 109708, Dec. 2023.
- [18] T. L. A. van den Heuvel, D. de Bruijn, C. L. de Korte, and B. van Ginneken, “Automated measurement of fetal head circumference using 2d ultrasound images,” *PLOS ONE*, vol. 13, no. 8, pp. 1–20, 08 2018.
- [19] S. Qiao, W. Shen, Z. Zhang, B. Wang, and A. Yuille, “Deep co-training for semi-supervised image recognition,” in *Proceedings of the European Conference on Computer Vision*, 2018.
- [20] X. Luo, M. Hu, T. Song, G. Wang, and S. Zhang, “Semi-supervised medical image segmentation via cross teaching between CNN and transformer,” in *Medical Imaging with Deep Learning*, 2022.